Is the transition impact to post-impact rock complete? Some remarks based on XRF scanning, electron microprobe, and thin section analyses of the Yaxcopoil-1 core in the Chicxulub crater

Smit, J.; van der Gaast, S.J.; Lustenhouwer, W.T.

published in
Meteoritics and Planetary Science
2004

DOI (link to publisher)
10.1111/j.1945-5100.2004.tb01132.x

document version
Publisher's PDF, also known as Version of record

Meteoritics & Planetary Science 39, Nr 6, 1–crossref to last page (2004)
Abstract available online at http://meteoritics.org

Is the transition impact to post-impact rock complete? Some remarks based on XRF scanning, electron-microprobe, and thin section analyses of the Yaxcopoil-1 core in the Chicxulub crater

J. SMIT,[1*] S. VAN DER GAAST,[2] and W. LUSTENHOUWER[1]

[1]Faculty of Earth and Life Sciences, Vrije Universiteit, de Boelaan 1085, 1081hv Amsterdam, Netherlands
[2]NIOZ, P.O. Box 59 NL-1790 AB Den Burg, Texel, Netherlands
[*]Corresponding author. E-mail: smit@geo.vu.nl

(Received 11 September 2003; revision accepted 15 March 2004)

Abstract–The transition from impact to post-impact rocks in the Yaxcopoil-1 core is marked by a 2 cm-thick clay layer characterized by dissolution features. The clay overlies a 9 cm-thick hardground, overlying a 66 cm-thick crossbedded unit, consisting of dolomite sandstone alternating with thin micro-conglomerate layers with litho- and bioclasts and the altered remains of impact glass, now smectite. The micro-conglomerates mark erosion surfaces. Microprobe and backscatter SEM analysis of the dolomite rhombs show an early diagenetic, complex-zoned, idiomorphic overgrowth, with Mn-rich zones, possibly formed by hot fluids related to cooling melt sheet in the crater. The pore spaces are filled with several generations of coelestite, barite, K-feldpar, and sparry calcite. XRF core scanning analysis detected high Mn values in the crossbedded sediments but no anomalous enrichment of the siderophile elements Cr, Co, Fe, and Ni in the clay layer. Shocked quartz occurs in the crossbedded unit but is absent in the clay layer. The basal Paleocene marls are strongly dissolved and do not contain a basal Paleocene fauna. The presence of a hardground, the lack of siderophile elements, shocked quartz, or Ni-rich spinels in the clay layer, and the absence of basal Paleocene biozones P0 and Pa all suggest that the top of the ejecta sequence and a significant part of the lower Paleocene is missing. Due to the high energy sedimentation infill, a hiatus at the top of the impactite is not unexpected, but there is nothing in the biostratigraphy, geochemistry, and petrology of the Yaxcopoil-1 core that can be used to argue against the synchroneity of the end-Cretaceous mass-extinctions and the Chicxulub crater.

INTRODUCTION

One of the main goals of the Chicxulub Scientific Drilling Program (CSDP) is to establish the relationship between the Chicxulub impact crater and the Cretaceous-Tertiary (K/T) boundary, in particular, the mass-extinction event at the K/T boundary. Therefore, complete recovery of the transition from impact to post-impact rock was of critical importance.

Hole Yaxcopoil-1 was drilled as the first part of the CSDP program. Yax-1 had three high-priority intervals within a limited depth of 1800 m: the post-impact filling of the crater, the impact rock sequence, and the target rocks (Dressler et al. 2003). To reach these units in a single hole within the limited drilling depth of Yax-1, a position was chosen between the Pemex drill hole Yucatan-6, 60 km from the center (Fig. 1), and the rim of the crater.

Only limited seismic information was available. Therefore, the Birps-1 Chic-1 line (Morgan et al. 2004) was rotated around the center of the crater and projected across Yax-1. Using hole Yucatan-6 (Yuc-6), that also intersected this rotated line, as reference, the depth of the impactites was correctly predicted, but the expected thickness of >800 m of ejecta was not recovered, presumably because either the ejecta was partially eroded from the Yax-1 locality (Dressler 2004) or not deposited because Yax-1 is located on top of a large megablock (Stoeffler 2004). The drilling logs of Pemex and a limited set of samples were available for well Yuc-6. From these data, one could infer a thickness of >20 m for transition from ejecta to post-impact infill (Fig. 3) that probably consists of material reworked by currents. Yaxcopoil-1 reached a depth of 1511 m, and recovered 1107 m continuously cored sequence from a depth of 404 to 1511 m below the rig floor. The Yax-1 core can be subdivided into three major and one minor units: the post-impact infill of the

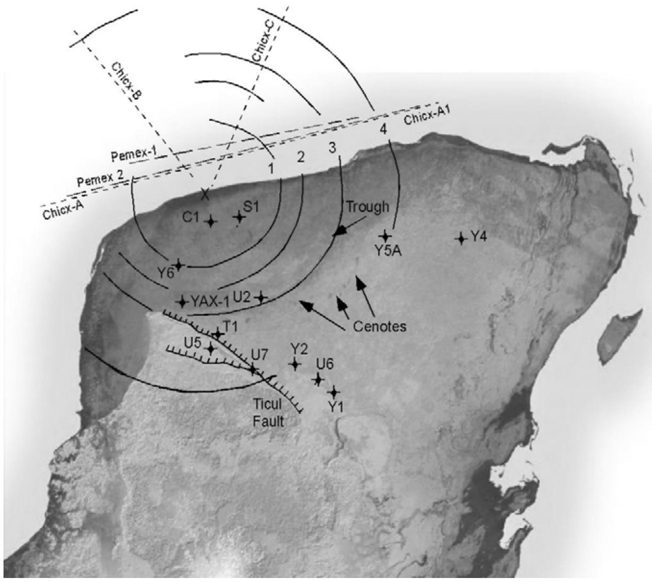

Fig. 1. Map showing the location of the Yaxcopoil-1 hole. The Pemex and UNAM holes and the rings of the Chicxulub crater gravity anomalies superimposed on a shuttle radar image are also shown. Photo courtesy of Mike Whalen.

crater (404–794.11 m), the impact ejecta (807.92–894.94 m), and the pre-impact rocks (894.94–1511 m). The interval 807.92–794.11 m represents the water-transported material in the crater just after the crater formation. In this interval, a conspicuous break from green, an altered glass-dominated interval to light crossbedded dolomite sandstone occurs at 794.75 cm. The analysis of the top of this transition of impact to post-impact rocks is the subject of this study.

The 75 cm-thick transitional core-segment (793.85–794.60 m) was cut with a thin diamond blade and split in two. One half was further cut into 107 samples to fulfill the sample requests of other investigators, which are reported in this special issue. We analyzed 40 split samples from the entire Yax-1 core, 20 from the core segment (samples 306 to 325), and performed an XRF scan on the unsampled half of the working half of the core. Of each of the 20 samples, polished thin sections were prepared for analysis of the sedimentary textures, foraminiferal content, mineralogy, cathode luminescence microscopy, scanning electron microscopy, and electron microprobe analysis. Unfortunately, it was not possible to prepare washed residues from the highly indurated samples. XRD spectra (XRPD) were obtained from a few samples to investigate the mineralogy. Stable isotope analyses were performed on bulk rock samples from carbonates below and above the impact rocks.

Interval 404–794.11 m: Impact Basin Infill

The Chicxulub crater formed a deep sea basin (>800 m; Morgan 2004) just after impact. This is compatible with the foraminiferal evidence (Arz et al. 2004). The interval 404–793.85 m represents the post-impact filling of the crater. The sequence is basically a hemipelagic deep-water sequence containing abundant, but badly preserved, planktic foraminifers and nannofossils.

The lithology from 404–600 m is dominated by episodic(?), perhaps rhythmic, alternations of laminated black shales and bioturbated light colored marls. Below 690 m depth, the sequence is interrupted by numerous mass flows. The laminated black shale intervals diminish downcore from 623.8 m, where an abrupt break may indicate a hiatus. The lowest clearly laminated interval is found at 740 m.

Sample YAX-1_452.8 yielded a nannofossil association (*Disocaster sublodoensis*, *D. barbadiensis, D. saipanensis, Chiasmolithus solitus, C. gigas*(?), *Reticulofenestra sp. R. bisecta, R. umbilica, Coccolithus formosus, Sphenolithus radians*) indicative of zone NP16 (43.5–40.2 Myr; Berggren et al. 1995) at 452.8 m (P. Ziveri, personal communication). The average sedimentation rate of the post-impact interval between 452.8 and 794.11 m, assuming that the lowest post-impact filling is the earliest Paleocene, is, therefore, between 13.5 and 15.5 m/Myr. The blackshale-limestone alternations are induced by episodic or periodic changes in oxygenation of the crater basin floor. These might correspond to Earth axis precession-induced climate changes, as is observed in hemipelagic Maastrichtian-Paleocene sections at this paleolatitude of 28°, like the Zumaya and Gubbio sections (Kate and Sprenger 1993; Scotese et al. 1988). If this is, indeed, the cause, one would expect, based on the overall sedimentation rate, to find a thickness of around 30 cm of a black-shale/limestone couplet. However, such thickness is not obvious from inspection of the core box photographs.

Suevitic Ejecta Interval

The interval 794.75–894.94 m represents a suevitic melt-rich breccia unit subdivided into six subunits (Dressler et al. 2003). The top 13.17 m of the suevitic interval (807.92–794.75 m) are extremely rich in dark green clay clasts, presumably glass altered to clay-minerals (smectite). The transition from indurated suevitic breccia with > to the glass-rich interval is sharp and marked by a drilling gap of <1.5 m between core runs 138 and 139 (Fig. 2). This top interval is considered reworked as the lithoclasts are relatively small and sorted. In addition, the interval is poorly lithified, indicating that the clasts were not welded together while still hot and plastic but were already cooled in seawater and loosely packed together. However, sedimentary features such as crossbedding or clear size grading were not observed, except at the very top from 794.74 to 794.11 m. This suggests reworking by initially extremely strong currents, linked to the catastrophic post-impact surge of water into the crater. It is not clear whether, and how much of, the suevitic breccias were removed from the Yaxcopoil location by this catastrophic surge.

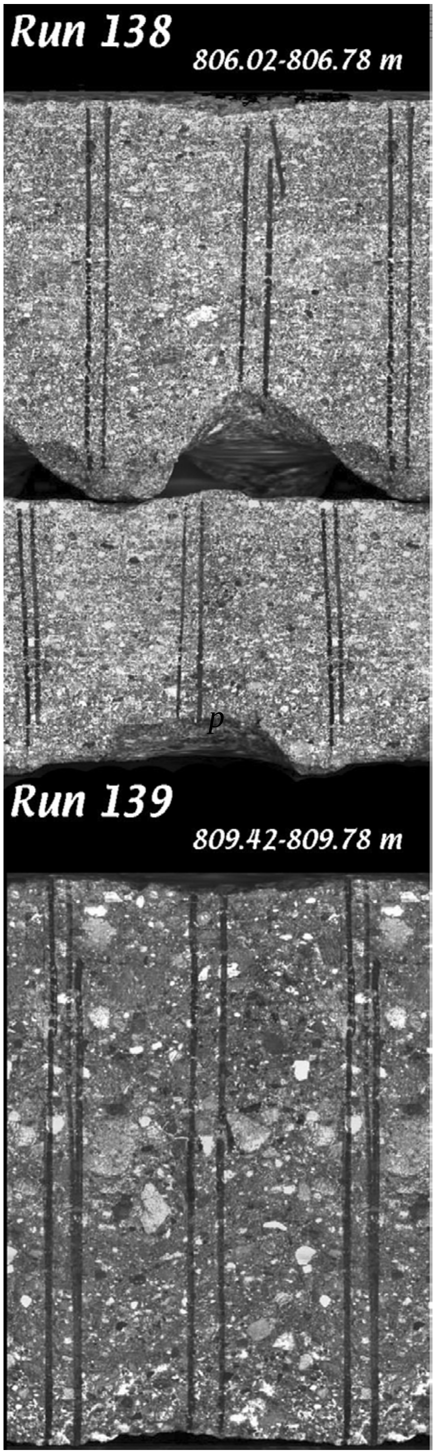

Fig. 2. Core-scanning (DMT® CoreScan) images of the transition from lithified clast-rich suevitic ejecta to loosely cemented, glass-rich, probably water transported ejecta at 79.

Pre-Impact Target Rocks

The interval 894.94–1511 m consists of carbonate platform and evaporitic rocks, dominantly poorly fossiliferous dolomites, anhydrites (27.2%), and other carbonate rocks, displaying a highly variable dip of the bedding planes. The variation in dip suggests that the drill core penetrated several superimposed mega blocks in different orientations that might have caused duplications in stratigraphy that cannot be resolved because of the lack of fossils. (Dressler et al. 2003). The crystalline Pan-African basement has not been reached.

Transition Impact to Post Impact Rocks

As stated above, one of the main goals of the CSDP project is to establish the relationship between the Chicxulub impact crater and the K/T boundary and its role in the extinctions at the K/T boundary. The core interval 793.85–794.73 m contains the critical transition from the impact to post-impact lithologies. The transition is visually sharp and marked by a dark 2 cm-thick clay layer at 794.11 m. (Fig. 3). It is tempting to equate this level to the K/T boundary, but that is not correct. According to the definition of the global stratotype definition (GSSP) of the K/T boundary (Cowie et al. 1989), the K/T boundary should actually be placed below the ejecta of the Chicxulub crater, assuming the Chicxulub crater is the source crater of the global ejecta layer (Smit 1999).

If Chicxulub is the source crater of the global ejecta layer, the sequence of post-impact lithologies in the crater should be comparable to other complete deep marine sections in a similar facies as the hemipelagic infill of the crater. Good examples of such sections occur near Agost and Caravaca in Spain and in eastern Mexico (Smit 1999). The lithological sequence of these sections outside the crater usually overlies a thick homogenous sequence of upper Maastrichtian marls that are rich in planktic foraminifers. This Maastrichtian sequence is abruptly overlain by an ejecta layer. Around the margins of the Gulf of Mexico, the ejecta are often mixed together with local (bio)clastic debris, presumably due to impact-triggered tsunami currents and mass flows. These layers typically contain tektite-like impact glass and limestone ejecta fragments at the base and an iridium anomaly, Ni-rich spinels, and shocked minerals at the top. The global ejecta layer forms a thin, 3 mm-thick, iridium, microkrystite, and shocked mineral enriched layer. This distal layer probably represents the global fallout of the impact vapor cloud (Smit et al. 1992). The thin ejecta level marks the mass-mortality and mass-extinction of most of the planktic foraminifers and other calcareous planktic biota. The ejecta are directly overlain by a 1–10 cm-thick layer of clay. This clay layer represents an ocean where primary productivity is very low, because it is characterized by a negative $\partial^{13}C$ excursion (Hsü and McKenzie 1985; Zachos et al. 1989). This clay layer corresponds to the foraminiferal P0 (zero) zone, or *Guembelitria cretacea* zone, because it contains remnants of a once diverse Maastrichtian calcareous planktic (foraminiferal and nannofossil) population. P0 is marked by the relative abundant occurrence of the foraminifer *G. cretacea* and, often,

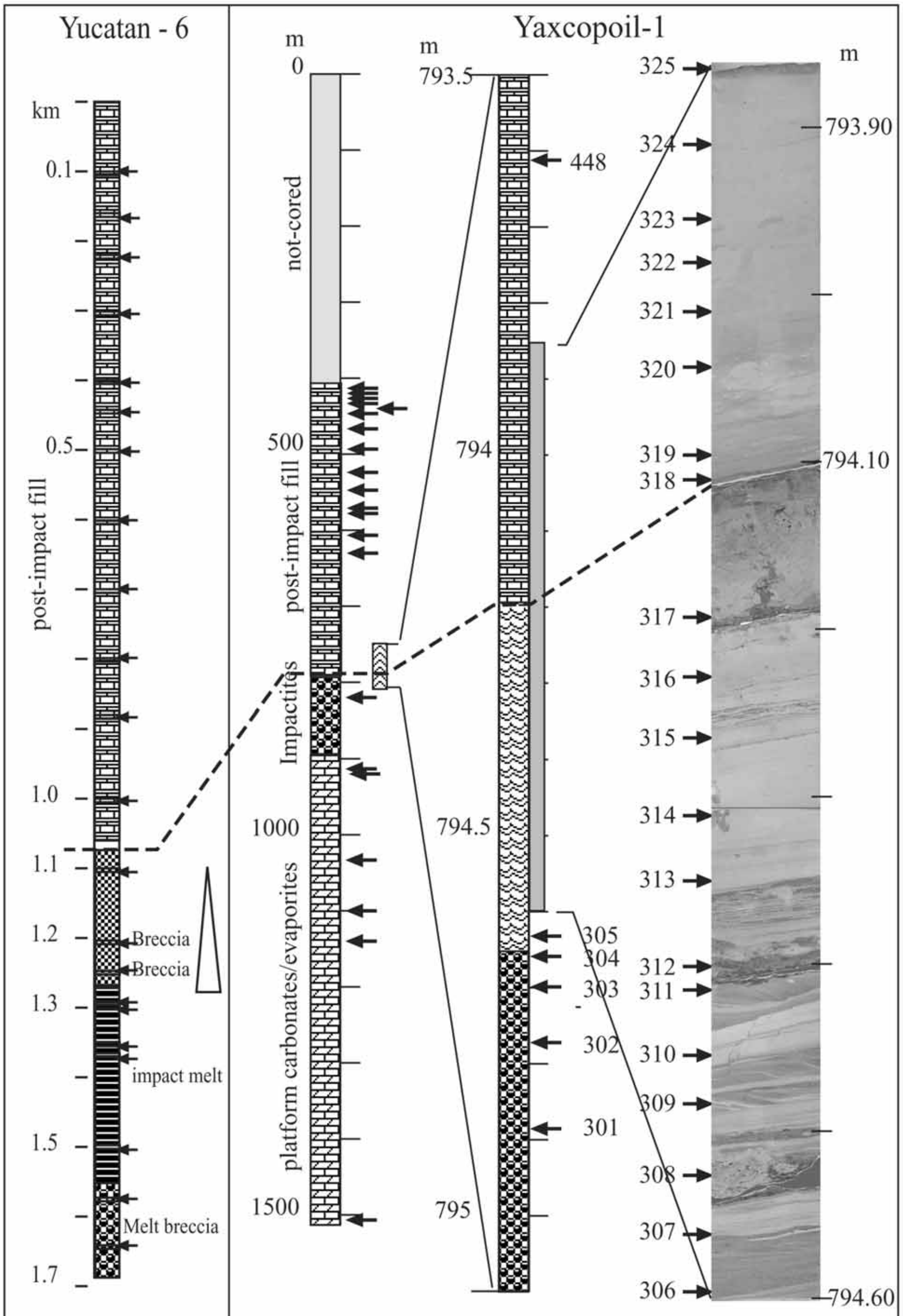

Fig. 3. Schematic lithologic representation of the Yaxcopoil-1 hole next to the litholog of the Yucatan-6 hole. Successive enlargement shows the position of core-segment 794.60–793.83 m. Sample numbers and locations are indicated (arrows). The depth is given in meters: a) melt and suevitic breccia; b) melt; c) breccia; d) hemipelagic crater infill; e) platform carbonates and evaporites; f) crossbedded dolomitic sandstone; g) base post-impact infill.

specimens of Cretaceous affinity that are either reworked from underlying strata or temporary survivors from the global impact event. The time span of P0 is estimated at about 10 Kyr (Smit 1999). The clay layer (P0 zone) grades into the next zone, known as the *P. eugubina* zone, P1a or Pa zone, depending on the definition of different foraminiferal workers. This zone is again rich in planktic foraminifers but characterized by very small unornamented foramineral tests that are very difficult to distinguish from one another, in particular, when the preservation is not good. The *P. eugubina* zone represents the adaptive radiation of the new Paleocene species after the adverse conditions of the P0 zone.

The expected Yaxcopoil-1 sequence might be comparable to this sequence outlined above. If the post impact filling is complete, and if the depositional environment were similar, one would expect to recover a clay layer similar to the P0 zone clay directly overlying the ejecta unit. The first post-impact infill of the crater would then provide a minimum biostratigraphic age of the crater.

RESULTS

Lithology

Core-segment 794.73–793.85 m can be divided into three distinct lithological units. The lower unit (794.73–794.19 m) includes crossbedded and parallel laminated fine-grained sands displaying low-angle cross-bedding representing climbing ripples. The ripples are interrupted by several coarse-grained layers that are rich in green smectite grains (see Fig. 3), a few bioclasts, and fragments of crystalline rocks, the quartz crystals of which often display planar deformation features (PDFs). The smectite grains contain internal cavities similar to altered impact glass fragments found around the crater (Schulte 2003) and similar to the altered glass in the suevitic ejecta. There is evidence for onlapping onto, and downcutting into, underlying layers of these coarse intervals that suggests interruption in sedimentation and erosion of underlying strata (Fig. 4). The dolomite sand grains display zoned idiomophic overgrowths of dolomite (Fig. 5). No evidence for isolated fossils was found in any of the 11 thin sections of the crossbedded interval, except within a few carbonate clasts. Arz et al. (2004) found a few reworked specimens in washed residues in this interval.

The second unit (794.19–794.11 m) probably represents a hard ground. The rock is strongly indurated. Several round, non-collapsed burrows filled with dolomite, crystalline lithoclasts, or smectite blebs can be observed. As all burrows in the overlying sediment are strongly compressed due to compaction, we suggest that the these burrows were either non-collapsed due to early lithification of the layer or have formed after lithification by boring by lithophagous organisms. Reworked bioclasts containing indeterminate foraminifers increase upward (Fig. 8c). The top 2 cm grades into a dark clay at 794.11–794.10 m (sample 318). This 3 cm interval displays an increasing number of horsetail laminations. Horsetail lamination is a typical dissolution feature in carbonate rocks, reminiscent of stacked stylolites. Such horsetail laminae are frequently visible in the dissolved topmost Cretaceous just below the K/T boundary, e.g., in the Stevns Klint section in Denmark (Christensen et al. 1973).

The third unit (794.10–793.85 m) is a finegrained, grey-green, micritic, marly limestone (wackestone). The lower

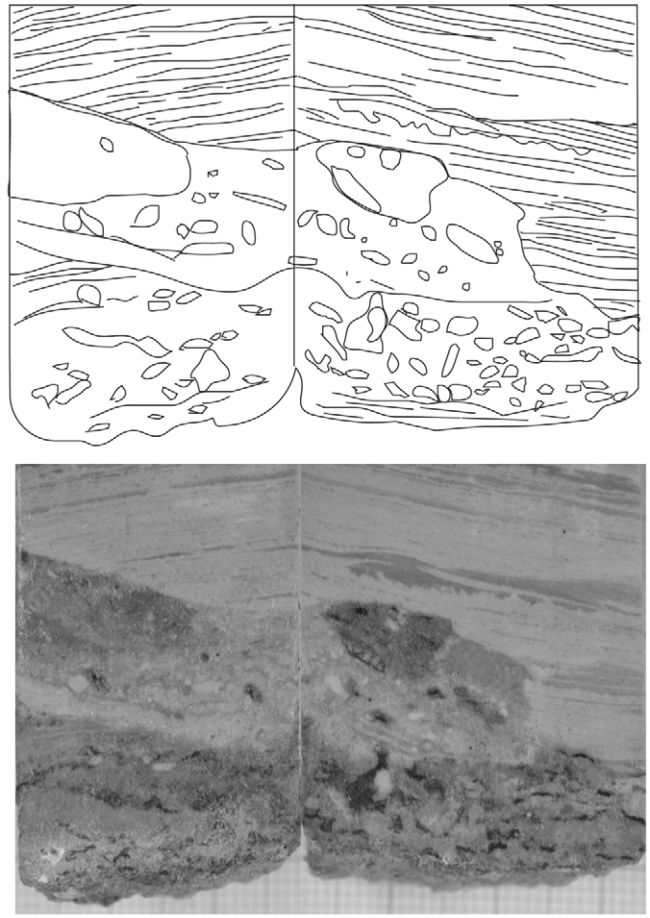

Fig. 4. Onlap of low-angle crossbedded dolomite sands on a lithified microconglomerate (794.4 m). The lithification might have existed before the onlap, indicating a hiatus at this level.

7 cm displays an upward decreasing number of horsetail laminae and contains residual concretions reminiscent of the dissolution features of the “ammonitico rosso” facies of the Appennines. The lower part is a poorly fossiliferous mudstone grading into a wackestone near the top that is rich in planktic foraminifers and calcareous dinoflagellates.

XRF Core-Scanning

The relative concentrations of Al, Si, K, Ti, Ca, Sr, Mn, Fe, Co, Cr, Ni, S, Cl, and Br were determined in the 75 cm-long unsampled core half using a second generation version of the CORTEX XRF core scanner (Jansen et al. 1998). Measurements were done with a step size of 1 mm, leading to a total of 750 analyses over the entire interval. The irradiated sample length was set at 1 mm in combination with a width of 10 mm. The counting time was 70 sec/step. The spectra were processed with software from Canberra (Winaxil 4.2.1). The results are given in Fig. 6. As the peaks were not calibrated with external standards, the measurements cannot be quantitatively interpreted yet. However, as each of the 750

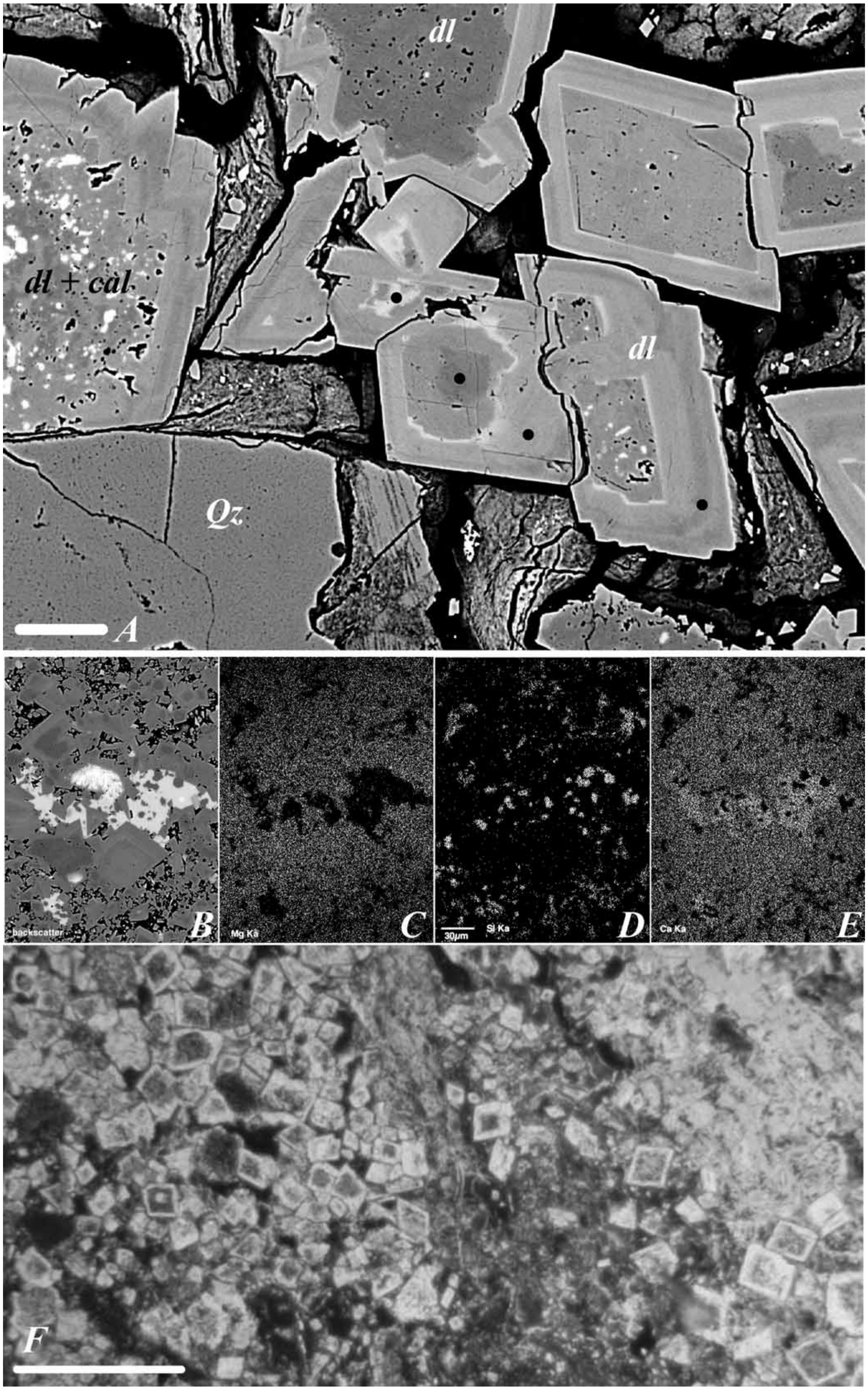

Fig. 5. SEM backscatter images of samples 312 (a) and 315 (b). Scale bar = 30 µm. The darker (Mg-rich) cores are idiomorphically first overgrown by Mn-rich dolomite (light band) and further by Mg-rich dolomite. Pore space is filled with smectite/glauconite. The black dots are locations of the electron microscopic analysis. Some dolomite cores display a spotty calcite (light) infilling. X-ray image maps of sample 315 are shown in 5c–5e: Mg (c); Si (d); and Ca (e). An image of dolomite crystals in sample 312 (bar = 500 µ) is shown in 5f.

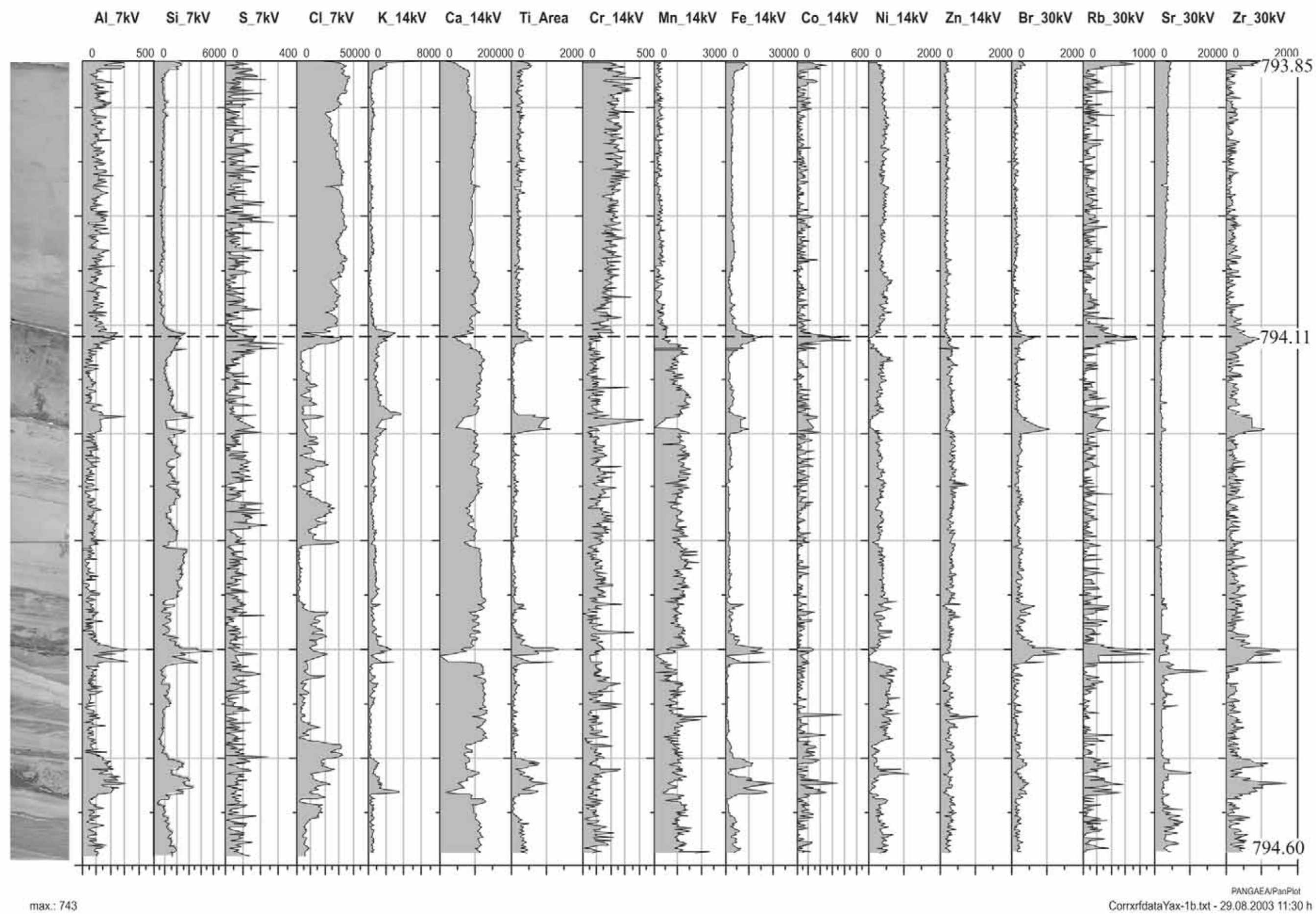

Fig. 6. Plots of the peak counts of 743 analyses of the elements detected by XRF core-scanning against the scanned core interval (left) (793.85–794.60 m, scale on the right). The core was scanned three times at 7, 14, and 30 kV, respectively. See text.

analyses were performed under identical circumstances, the peak heights of each element can be compared between samples, and the relative peak heights should faithfully reflect the relative concentrations in each analysis.

The layers rich in altered impact glass, now smectite, show peaks in Al, Si, Ti, K, and Fe. Sr displays erratic peaks in the reworked ejecta intervals, probably related to coelestine. The crossbedded and hardground intervals are characterized by slightly higher amounts of Ca and Mn (see also Figs. 5c–5e) The micritic post impact crater fill is relatively rich in Sr, Ti, Fe, and particularly, Cr. The clay layer at 794.11 m is not significantly enriched in siderophile elements, except in Co. Ni and Cr are depleted in the clay, while Cr is one of the elements that is invariably enriched along with Ir in the global K/T boundary ejecta layer.

Electron Microprobe

Thirty-three mineral phases were analyzed in three samples (311, 312, 318) by electron microprobe (EM). They were analyzed using a JEOL JXA-8800M electron microprobe operated at a voltage of 15 KeV and a current of 25 nA. The beamspot was set at 10 µm, and mineral and artificial standards were used for calibration. Samples 311 (794.42 m) and 312 (794.40 m) are from the dolomitic crossbedded sands, and sample 318 is from the clay layer at 794.12 m. (Table 1). X-ray maps of sample 315 were prepared to demonstrate the distribution of the elements in the crossbedded unit. In the pore-space between the dolomite rhombs, sparry calcite has grown as the latest phase, enclosing an idiomorphic authigenic quartz phase (Figs. 5b–5e). The sparry calcite makes bulk-sample stable isotope analyses of this interval unreliable because it remains unknown from which source the sparry calcite has been derived.

Samples 311/312

Small (<300 µm) dolomite rhombs consisting of a homogenous core with a zoned idiomorphic overgrowth (Figs. 5 and 7f) are the principal component (>98%) of the crossbedded layers. Most cores of the dolomite rhombs are rounded. Some of the cores show a sieve-like calcite infilling (Figs. 5 and 7g). This is unusual in a normal carbonate

Table 1a. Electron microprobe analysis of dolomite rhombs in sample 312.

	Calcite 311aeCal	Dolomite 311aaDlc	Core 312Dlc	Rim 1(Mn) 312Dr1	Rim 2 312Dr2	Rim 3 312Dr3
CaO	56.0	33.4	31.7	32.6	31.9	31.9
SrO	0.0	0.0	0.0	0.0	0.0	0.0
MgO	0.5	20.6	20.7	18.2	19.6	20.1
MnO	0.2	0.0	0.0	2.8	0.5	0.3
FeO	0.1	0.0	0.0	0.1	0.1	0.2
NiO	0.0	0.0	0.0	0.0	0.0	0.0
CO_2	44.0	47.8	47.8	47.8	47.8	47.8
Total	100.9	101.8	100.3	101.5	100.0	100.2

Table 1b. Electron microprobe results from sample 318.

	Spinel 318Chr	Titanite 311daTtn
SiO_2	0.1	31
TiO_2	0.7	35
Al_2O_3	16.6	2
V_2O_3	0.1	–
Cr_2O_3	36.6	0
Fe_2O_3	0	1
FeO	28.2	–
MnO	0.3	0
MgO	10.0	0
NiO	0.3	0
CuO	0.3	29
ZnO	2.3	–
CaO	0.5	–
Total	95.9	98

sedimentary environment but can be explained by exsolution upon heating of the grains, presumably by the thermal effects of impact. The zoned overgrowths are fairly complex compositionally (Figs. 5 and 7c). The initial overgrowth is enriched in Mn (up to 2.8%). The outer layers contain, in general, less Mg than the cores of the grains. The thickness of the overgrowths and their compositional trends are similar in all the grains. A slight upcore shift of the XRD peak from 2.894 å to 2.902 å suggests a slight change in the Ca/Mg ratio of the dolomite, but that is not apparent from the EM analyses of core and the rims of the individual dolomite crystals.

The next most abundant phase is hydrated phyllosilicate blebs (<4 mm) often concentrated in thin, coarse laminae between the crossbedded dolomite sand ripples (Fig. 7g). The structure of the blebs is very similar to the altered impact glasses from Beloc, Haiti, and eastern Mexico. These blebs contain the remains of spherical cavities, now often filled by either pure calcite or a poorly crystallized smectite. In Beloc, it can be demonstrated that these clay mineral grains with cavities are the alteration products of vesicular impact glass (Izett 1991). We infer, therefore, that the green Yax-1 grains are similar alteration products of impact glass. The XRD peaks (CuKa 2θ) (Fig. 8) of the green grains show it is a smectite, although the chemical composition is more comparable to glauconite because it contains up to 6.8% K_2O. (Table 1). We assume that by analogy to the smectite-glauconite grains (altered microkrystites; Montanari 1990) at the K/T boundary in Italy, the glauconite is the more crystalline clay mineral end member of the alteration process of Chicxulub glass.

Complex lithoclasts contains fragments of quartz, titanite, apatite, albite and plagioclase, phlogopite, and a few zoned garnets. Some of these minerals display deformation structures, like bending of twin lamellae, and about 20% of the quartz display planar deformation features (PDFs) (Fig. 9a), indicative of shock. These grains are most likely derived from the crystalline basement of Chicxulub. Some carbonate fragments contain cross sections of benthic foraminifers. Rare chalcopyrite and pyrite occur in detrital grains. They are sometimes associated with anhydrite (Fig. 7i), suggesting derivation from the evaporitic target rocks. Sparry calcite often fills interstitial spaces between the rhombs, but the filling is not complete. About 50% of the pore space is not filled by authigenic minerals. Idiomorphic K-feldspar occurs within the calcite and is, thus, crystallized slightly before the sparry calcite infilling. Zoned barite/coelestine intergrowths also fill the porespace. As calcite grows around the barite, the barite predates calcite infilling. The presence of coelestite probably explains the erratic Sr peaks in the XRF scan.

Sample 318

The principal component is a clay mineral matrix, with many floating dolomite rhomb fragments, often with irregular outlines due to dissolution. These fragments display identical zoning as the rhombs from the underlying unit. Some enclosed blebs of green clay have the same glauconitic composition and texture as those in 311/312. Several sublayers contain crystalline clasts and separate dolomite clasts, some filled with fossil fragments. An interesting type of clast is compositionally and texturally identical to the cross-ripple beds just below (Fig. 7c), suggesting that the ripple beds were lithified and eroded before deposition of the clay layer of sample 318. Scattered through the sample are numerous fragments of a S-rich apatite, clearly fish remains (Fig. 7b). A single grain of chromite was found (Fig. 7h). This grain is not comparable to the Ni-rich spinels frequently found at the K/T boundary because of the high Zn (2.3% ZnO) and low Ni (<0.27% NiO) content. In contrast to the samples below (311/312), not a single grain with PDFs has been found among the numerous quartz grains present.

Table 1c. Electron microprobe analyses of smectite/glauconite, kspar, albite, and plagioclase.

Sample	Glauconite? 311bGlta	Glauconite 318bGlt	Glauconite 312bGlt3	Kspar 311aeKfs	Albite 311daAbb	Plagioclase 318dPl
SiO_2	51.5	51.2	51.4	66.2	68.9	55.1
TiO_2	0.3	0.2	0.2	–	–	–
Al_2O_3	14.9	10.9	13.8	17.7	19.3	28.1
Cr_2O_3	0.0	0.0	0.0	–	–	–
FeO	4.7	10.6	8.5	–	–	–
Fe_2O_3	–	–	–	0.0	0.1	0.5
MgO	5.5	6.7	6.2	–	–	–
NiO	0.0	0.0	0.0	–	–	–
CaO	0.9	1.1	1.3	0.4	0.3	10.4
SrO	–	–	–	0.0	0.0	0.2
Na_2O	0.9	0.6	0.9	0.0	10.9	5.1
K_2O	2.1	6.5	5.4	16.4	0.4	0.3
BaO	–	–	–	0.0	0.0	0.1
F	0.3	0.3	0.3	–	–	–
Cl	0.9	0.3	0.7	–	–	–
O_F_Cl	0.3	0.2	0.3	–	–	–
Total	81.7	88.1	88.5	100.7	99.9	99.7

Table 1d. Electron microprobe results from sample 312.

	Apatite 318	Coelestite 312	Barite 312
SiO_2	0.2	–	–
La_2O_3	0.1	–	–
Ce_2O_3	0.2	–	–
Nd_2O_3	0.1	–	–
FeO	0.3	–	–
MnO	0.1	–	–
CaO	55.2	0.4	0.4
SrO	0.1	34.7	2.4
BaO	–	24.9	63.5
Na_2O	0.1	–	–
P_2O_5	41.1	40.3	34.2
SO_3	0.2	–	–
F	3.3	–	–
Cl	0.3	–	–
O_F_Cl	1.5	–	–
Total	102.8	100.4	100.5

Biostratigraphy

Thirteen thin sections from the interval 794.60–794.11 m were analyzed for planktic foraminifers. Except for a few benthic foraminifers in reworked dolomite fragments, we did not find isolated specimens. Arz et al. (2004) report a few reworked Cretaceous specimens.

Eight thin sections from the interval 794.10–793.03 m were studied to establish the age of the first post-impact Paleocene infill. Sample 319 from the top of the clay layer does not contain any recognizable foraminifers. Sample 320 (5 cm higher) contains a poorly preserved fauna. The tests are small, thin-walled, and strongly dissolved, and most of the foraminiferal tests are small and thin-walled, comparable to faunas from the *P. eugubina* zone and the base of the *S. pseudobulloides* zones in the sub-equatorial oceans. Tests of *Eoglobigerina spp.*, *Chiliguembelina sp.*, and a few small *S. pseudobulloides* were recognized. The faunas in samples 447 and 448 are slightly better preserved yet contain essentially the same faunal elements, but these samples also show a high abundance of *Thoracospheara operculata* (Fig. 9d). This calcareous dinoflagellate species is well-known to form acmes at the base of the Paleocene, particularly in the *P. eugubina* and *S. pseudobulloides* zones.

Faunal elements from both the P0 zone (*G. cretacea*) and the *P. eugubina* (Pa) zone seem to be missing. In none of the eight thin sections above level 794.11 m were specimens of Cretaceous affinity found.

DISCUSSION

Interval 793.85–794.60 is one of the most disputed intervals of the Yaxcopoil-1 core.

On first inspection of the core, it seemed that this interval contained the classical elements of the K/T boundary: an ejecta layer overlain by a few cm-thick clay layer followed by the first Paleocene pioneering foraminiferal faunas. Yax-1 may also provide the means to test the hypothesis that several Cretaceous species survived the K/T event. Additionally, the suggestion that the Chicxulub crater may actually precede the K/T boundary event by approximately 300 Kyr (Keller et al. 2002) might be tested on Yax-1, provided that all classical K/T criteria are present. But, is the Yax-1 section really complete? Several lines of evidence indicate that it is not. Therefore, the Yax-1 drill core cannot be used to test the above mentioned hypotheses. The crossbedded interval from 794.60–794.19 cm contains several levels (at 794.52 and 794.40 m) where overlying crossbedded sediments onlap on a previously lithified surface. This suggests a hiatus at these

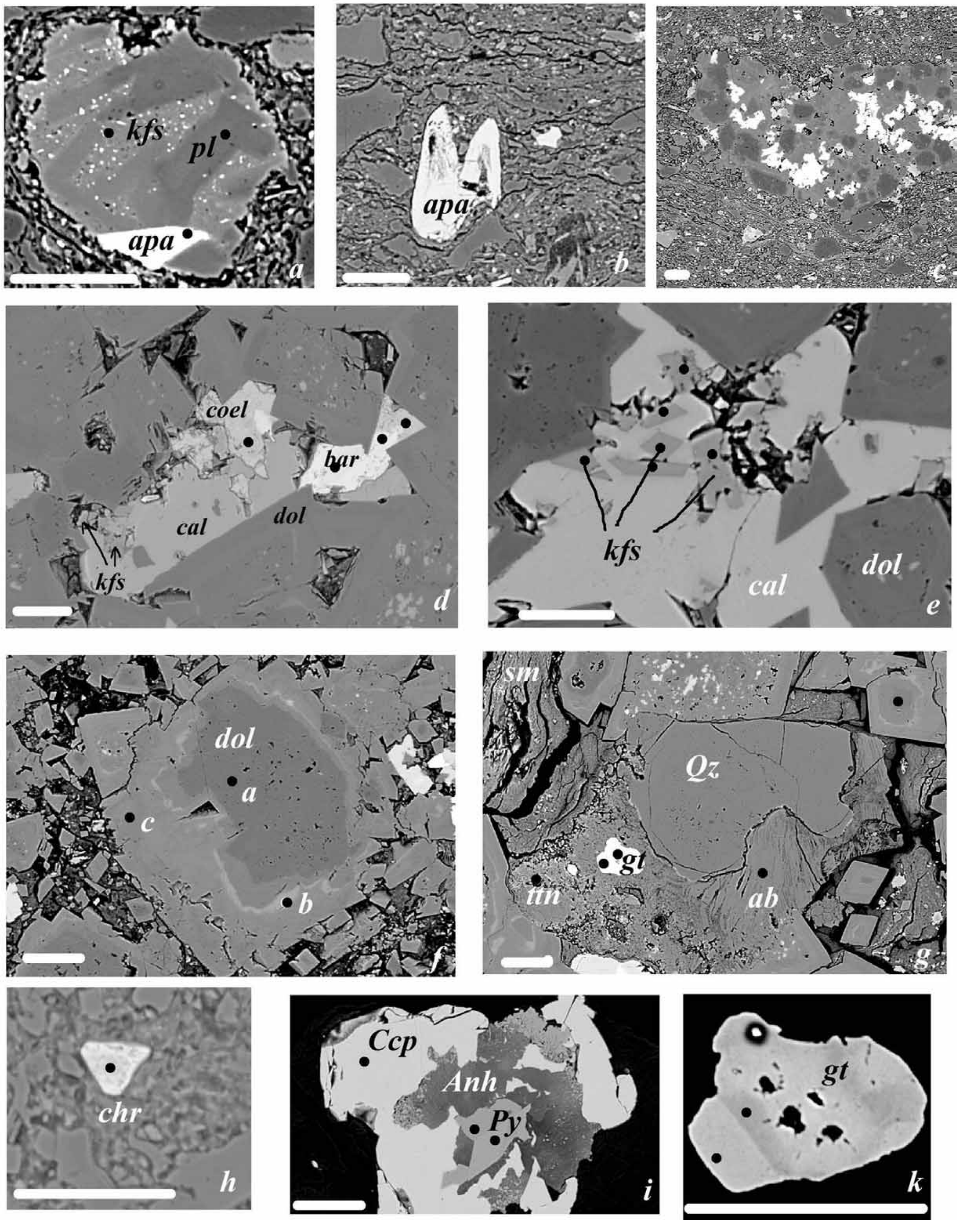

Fig. 7. Backscatter SEM images of various mineral phases in the interval impact to post-impact rocks. All scale bars = 30 µm. The black dots are spots of electron microsope analysis: a) lithic fragment (sample 318) with plagiolase, k-feldspar, and apatite; b) "s"-rich apatite, one of the many fish remains in 318; c) fragment similar to the underlying dolomitic sand in sample 318, indicating that the crossbedded sands of 794.60–794.19 m were lithified and eroded before deposition in the clay (794.11 m); d) pore infilling of the porous dolomitic sands by coelestite, barite, k-feldspar, and calcite (312); e) idiomorphic k-feldspar crystals enclosed in calcite. Sample 312: f) dolomite crystal with zoned overgrowths; a–c) see Table 1; g) metamorphic lithic fragment in sample 311 containing garnet (gt), titanite (ttn), albite (ab), and quartz (Qz). The albite shows bending of twin-lamellae. Sm = smectite; h) idiomorphic chromite grain in sample 318; i) clast containing chalcopyrite (ccp) and pyrite (py) replacing anhydrite (anh); k) an enlargement of 7 g.

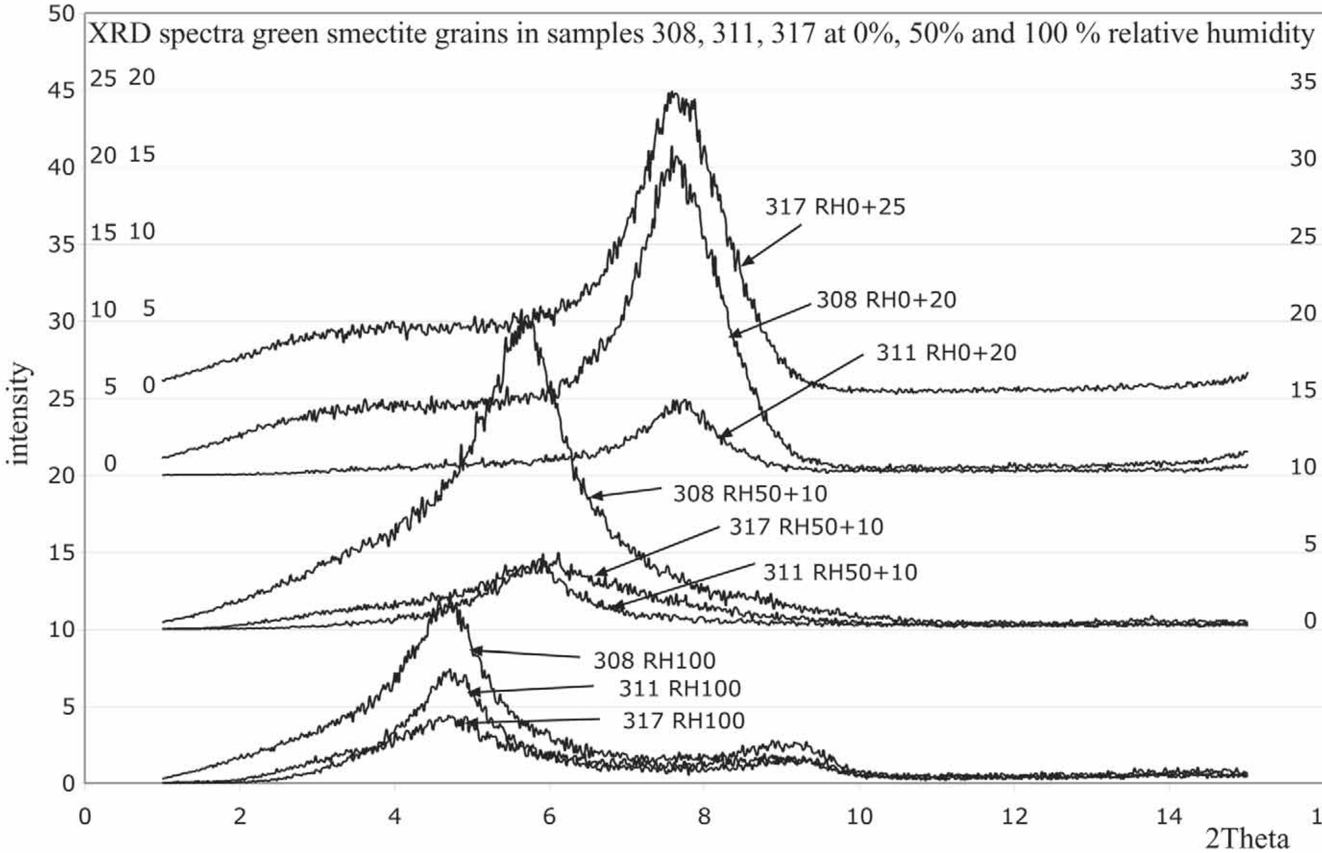

Fig. 8. XRD 2θ peaks of smectite grains in samples 308, 311, and 317 at different relative humidities (0%, 50%, and 100%). EM analyses of these smectites are in Table 1.

levels. Interval 794.19–794.11 m has all the aspects of a hardground surface. Several burrows are round and non-compressed, suggesting that they were made by lithofagous borers after lithification and remained open when they were filled by clay and fragments of green clay blebs and dolomite clasts. The overlying 2 cm-thick clay layer seems to be a residual clay, left after dissolution of carbonate. The typical horsetail laminae, similar to stylolites, suggest strong dissolution, and the abundance of fish remains also suggests the presence of an omission surface that is often enriched in residual fish debris.

The clay layer itself, if comparable to the global K/T boundary clay, would be enriched in siderophile elements, Ir, Ni, Co, Fe, Cr, and might contain microkrystites, Ni-rich spinels, and shocked crystals. Stuben et al. (2004) have shown that the platinum group elements are not enriched in the clay layer. The XRF analyses presented in this study do not show a significant enrichment in Ni, Fe, and Cr in the clay, while these elements, in particular Cr, are invariably enriched together with Ir in the iridium-rich boundary clay. Although many quartz crystals were encountered in the clay layer, none of these display PDFs. We have searched the clay layer for evidence of Ni-rich spinels, which are often present in the K/T boundary clay, but found none, except one grain of chromite. But, its chemical composition is not compatible with typical Ni and Cr-rich spinels at the K/T boundary (Kyte and Smit 1986).

These lines of evidence suggest that the clay is a residual clay, overlying a hardground surface, both indicative of a significant hiatus rather than being the equivalent of the K/T boundary clay. The magnitude of the hiatus is difficult to assess. The foraminifers in the first post-impact background infill are strongly dissolved, and the interval may be condensed. The first recognizable foraminifers belong to the *P. eugubina* zone or *S. pseudobulloides* zone, up to 2 Myr after the K/T event. Goto et al. (2004) found specimens of *Thoracosphaera*, *Braarudosphaera*, and small *Cruciplacolithus primus* in sample 793.94, suggesting an age younger than 64.8 Myr (Berggren et al. 1995). Rebolledo et al. (2004) have shown that, 11 cm above the clay layer, a magnetic reversal is present, which might represent the C29R-C29N reversal. C29R-C29N is estimated to occur 330 Kyr above the K/T boundary (Berggren et al. 1995), which sets the upper limit of the hiatus. Removal of a significant part of the top of the ejecta deposits would not result in a significant time hiatus, as the ejecta are, geologically speaking, all the same age. The 11 cm-thick hardground interval appears, therefore, either extremely condensed or the hiatus represented in the hardground lasted a maximum of 330 Kyr.

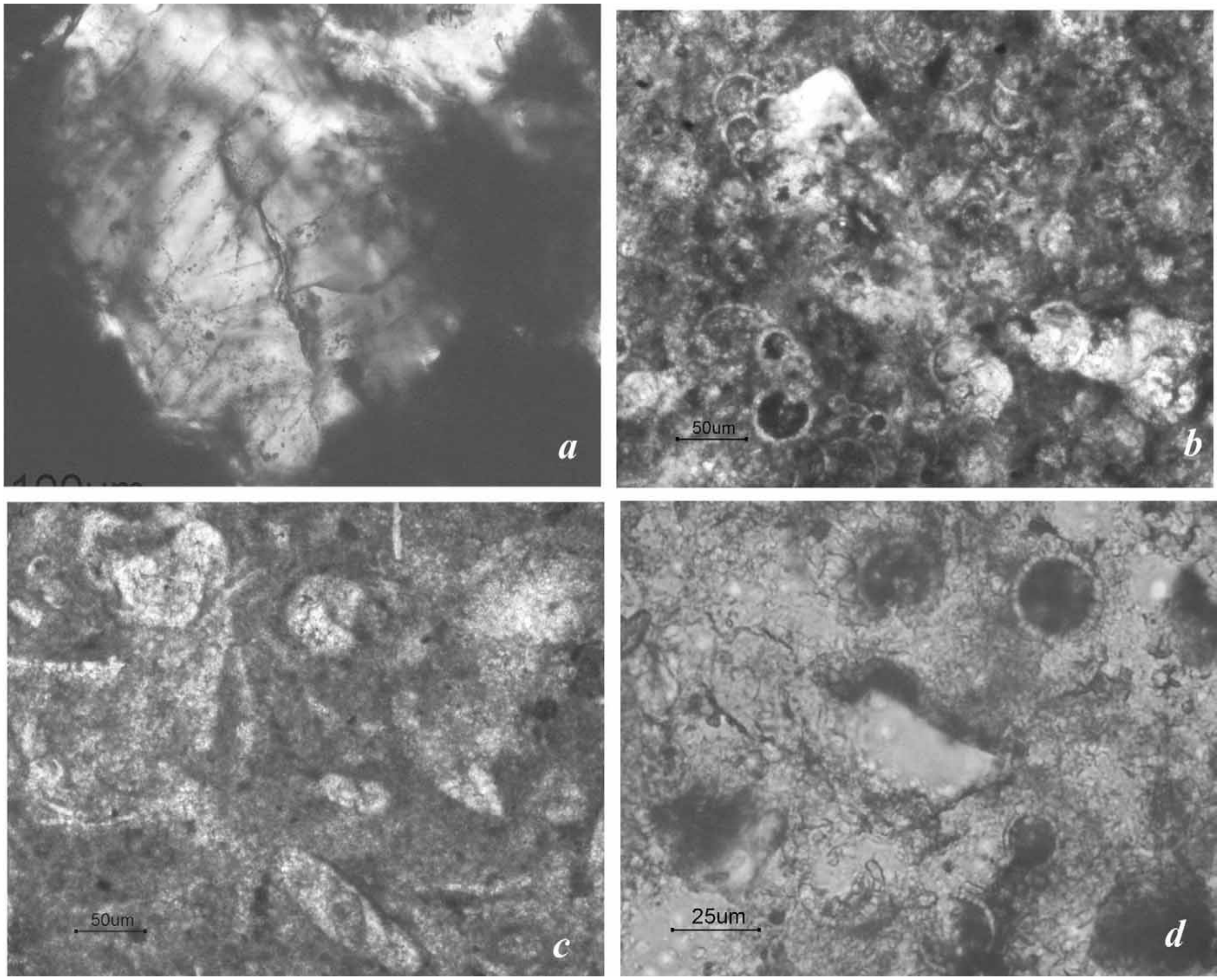

Fig. 9. Thin sections of impact (a, c) and post impact (b, d) intervals: a) quartz with PDFs in sample 312. About 50% of the grains in the sample show PDFs; b) sample 320, earliest Paleocene fauna, about 6 cm above the hardground. Thin-walled tests of *Eoglobigerina sp.* and *Chiloguembelina sp.* and absence of *P. eugubina* suggest an age of P1a, 70–470 Kyr post-K/T boundary (Berggren et al. 1995); c) fragment of limestone with numerous indeterminate benthic foraminifers, sample 318; d) abundant *Thoracospaera* tests in sample 325 (793.85 m) blooms of *Thoracospaera* are characteristic of lower Paleocene Palpha-P1a zones.

But, can the Chicxulub impact predate the K/T boundary by about 300 Kyr? The hypothesis was raised by Stinnesbeck et al. (2001) on the basis of putative spherule layers below the K/T boundary in Mexico and Haiti. However, these sections in the Gulf of Mexico region are invariably disturbed, and no evidence for two layers has been found anywhere outside disturbed sections in the Gulf of Mexico. Thus, explanations such as tsunami wave reworking, slumping, or multiple mass-flows remain the preferred alternatives for the repetition of spherule layers. Since part of the top of the ejecta sequence in Yax-1 is eroded, and a hiatus of up to 330 Kyr is present at the top of the ejecta, the hypothesis Stinnesbeck et al. (2001) cannot be accepted or rejected on the basis of Yax-1 data. The suggestion by Keller et al. (2004) that the crossbedded interval 794.6–794.11 contains an indigenous Cretaceous planktic fauna is highly unlikely for several reasons: 1) we did not find Cretaceous taxa but found zoned dolomite rhombs instead. Arz et al. (2004) found just a few badly preserved specimens in samples from the same levels. The size of the rhombs and the thickness of the zonal overgrowth of the dolomite rhombs is comparable to the thickness of a foraminiferal shell, creating the illusion of foraminiferal shells when two adjacent dolomite rhombs are positioned together; and 2) even if Cretaceous taxa are present, their presence within crossbedded sandstone layers suggests that they are reworked from older units, and therefore, they cannot be used for a biostratigraphic age. Other arguments that the Chicxulub crater is the one that deposited the iridium-rich layer precisely at the K/T boundary are circumstantial. The age dating of the impact melt sheet samples of the Chic-1 core in the center of the crater and the impact glass spherules at the K/T boundary in Haiti and Mimbral, Mexico (Swisher et al. 1992) demonstrated that the Ar/Ar age of the impact melt sheet and spherules at the K/T boundary in Haiti and Mimbral, Mexico are within error (100 Kyr) of the same age, the error being on the order of 100 Kyr not 300 Kyr. Also, the provenance age of shocked zircons (Bohor et al. 1992; Kamo et al. 1995) in Ir-rich ejecta layers shows that these are derived from a ~500 Myr old basement, compatible with the Pan-African basement underlying the Chicxulub crater. The best evidence for a single impact is probably the occurrence in many coal-swamp localities from Saskatchewan to New Mexico of the iridium layer with abundant shocked quartz and zircon, invariably directly on top of a layer containing spherules and splash-form grains. These spherules are morphologically indistinguishable from the spherules in Beloc, Haiti, and Mimbral (Bohor and Glass 1995). Even a single season of falling leaves would leave a recognizable layer of coal between the two impact layers, but there is none. A time span of 300 Kyr would certainly have left a substantial deposit between the two layers.

A hypothesis launched by Keller (1988) and repeated many times since holds that most Cretaceous species survived the K/T boundary event. The controversy was a side issue in the El Kef blind test (Ginsburg 1997) but could not be tested then because the possibility of extensive reworking could not be excluded.

The Chicxulub Paleocene crater-fill sequence seemed to be the golden opportunity to test the hypothesis of survivors again because there is no planktic foraminifer-bearing Maastrichtian sediment directly below the basal Paleocene, and therefore, reworking should be extremely unlikely. Reworking from the rim of the crater and the surrounding area would not provide reworked Maastrichtian planktic foraminifers either because those platform carbonate and lagoonal/evaporite sediments, likewise, do not contain these planktic tests.

Unfortunately, the hiatus at the top of the ejecta sequence precludes a definitive test. Although not a single Cretaceous foraminiferal test was found in the clay layer at 794.11 m or above, the strata that would hold the presumed survivors are missing. This test will await future CSDP drilling at a position where the chances for erosion and slumping are minimal, presumably in the very center of the central uplift near Chicxulub itself. Although, it is questionable whether a complete, well-preserved Paleocene section can be recovered anywhere in the crater, considering the pervasive hydrothermal alterations.

CONCLUSIONS

The transition from impact ejecta to post-impact basin infill is marked by a 62 cm-thick crossbedded unit that may reflect the last phases of the catastrophic infill of the basin.

The crossbedded unit is capped by a hardground followed by a residual clay. The clay is not enriched in siderophile elements or shocked quartz of Ni-rich spinels and is, therefore, distinct from the global K/T clay layer.

A hiatus of at most 330 Kyr is present between impact ejecta and high-energy sediments associated with crater infilling and the post-impact basin fill. This implies that a test of the relative age of the crater and the K/T boundary, as well as a test of the hypothesis of the existence of a substantial survivor population of planktic foraminifers, is unresolved. However, there is nothing in the biostratigraphy, geochemistry, and petrology of the Yaxcopoil-1 core that can be used to argue against the synchroneity of the end-Cretaceous mass-extinctions and the Chicxulub crater.

The crossbedded unit displays a complex history of dolomite crystal overgrowth and pore-space filling that may be caused by hydrothermal activity following the impact. The diagenetic sequence starts with overgrowth of dolomite, followed by a Kspar, coelestine/barite, and calcite, respectively, infilling of the pore space.

Acknowledgments–We thank A. van der Vaars and R. Gieles for assistance with the XRF core-scanning. Reviews by F. Hörz and T. Bralower are greatly acknowledged. This research was supported by a grant from the Vrije Universiteit. This is NSG publication 2004.03.03.

Editorial Handling—Dr. Philippe Claeys

REFERENCES

Arz J. A., Alegret L., and Arenillas I. 2004. For aminiferal biostratigraphy and paleoenvironmental reconstruction at Yaxcopoil-1 drill hole (Chicxulub crater, Yucatan Peninsula). *Meteoritics & Planetary Science* 39:???–???.

Berggren W. A., Kent D. V., Swisher C. C., III, and Aubry M. P. 1995. A revised Cenozoic geochronology and chronostratigraphy. In *Geochronology, time scales, and global stratigraphic correlation,* edited by Berggren W. A., Kent D. V., Aubry M. P., and Hardenbol J. Special publication 54. Tulsa: Society for Sedimentary Geology. pp. 129–212.

Bohor B. F. and Glass B. P. 1995. Origin and diagenesis of K/T impact spherules—From Haiti to Wyoming and beyond. *Meteoritics* 30:182–189.

Bohor B. F., Krogh T. E., and Kamo S. L. 1992. U-Pb isotopic ages of the K/T impact event and its target rocks from shocked zircons. *Meteoritics* 27:205.

Christensen L., Fregerslev S., Simonsen A., and Thiede J. 1973. Sedimentology and depositional environment of lower Danish fish clay from Stevns Klint, Denmark. *Bulletin of the Geological Society of Denmark* 22:193–212.

Cowie J. W., Zieger W., and Remane J. 1989. Stratigraphic Commission accelerates progress, 1984-1989. *Episodes* 112:79–83.

Dressler B. O., Sharpton V. L., Morgan J., Buffler R., Moran D., Smit J., Stöffler D., and Urrutia-Fucugauchi J. 2003. Investigating a 65 Ma old smoking gun: Deep drilling of the Chicxulub impact structure. *EOS Transactions* 84:125–130.

Dressler B., Schwandt C., Sharpton V., and Ames D. 2004. Impactites of the Yaxcopoil-1 drilling site, Chicxulub Impact Structure-

Petrography, geochemistry, and depositional environment. *Meteoritics & Planetary Science.* This issue.

Ginsburg R. N. 1997. An attempt to resolve the controversy over the end-Cretaceous extinction of planktic foraminifera using a blind test. Introduction: Background and procedures. *Marine Micropaleontology* 29:67–68.

Goto K., Tada R., Tajika E., Bralower T. J., Hasegawa T., and Matsui T. 2004. Evidence for ocean water invasion into the Chicxulub crater at the Cretaceous/Tertiary boundary. *Meteoritics & Planetary Science.* This issue.

Hsu K. J. and McKenzie J. 1985. A "Strangelove" ocean in the earliest Tertiary. In *The carbon cycle and atmospheric CO_2: Natural variations from Archean to the present,* edited by Sundquist E. T. and Broecker W. S. Washington D.C.: American Geophysical Union. pp. 487–492.

Izett G. A. 1991. K-T boundary tektites from near Beloc, Haiti. 22nd Lunar and Planetary Science Conference. pp. 625.

Jansen J. H. F., Van der Gaast S. J., Koster B., and Vaars A. J. 1998. CORTEX: A shipboard XRF-scanner for elemental analyses. *Marine Geology* 151:143–153.

Kamo S. L. and Krogh T. E. 1995. Chicxulub crater source for shocked zircon crystals from the Cretaceous-Tertiary boundary layer, Saskatchewan: Evidence from new U-Pb data. *Geology* 23: 281–284.

Kate W. G. T. and Sprenger A. 1993. Orbital cyclicities above and below the Cretaceous/Paleogene boundary at Zumaya (N Spain), Agost and Relleu. *Sedimentary Geology* 87:69–101.

Keller G. 1988. Biotic turnover in benthic foraminifera across the Cretaceous/Tertiary boundary at El Kef, Tunisia. *Palaeogeography, Palaeoclimatology, Palaeoecology* 66:153–171.

Keller G., Adatte T., Stinnesbeck W., Affolter M., Schilli L., and Lopez O. J. G. 2002. Multiple spherule layers in the late Maastrichtian of northeastern Mexico. In *Catastrophic events and mass extinctions: Impacts and beyond,* edited by Koeberl C. and MacLeod K. G. Boulder: Geological Society of America. pp. 145–161.

Keller G., Adatte T., Stinnesbeck W., Rebolledo-Vieyra M., Fucugauchi J. U., Kramar U., and Stuben D. 2004. Chicxulub impact predates the K-T boundary mass extinction. *Proceedings of the National Academy of Sciences* 101:3753–3758.

Kyte F. T. and Smit J. 1986. Regional variations in spinel compositions: An important key to the Cretaceous/Tertiary event. *Geology* 14:485–487.

Montanari A. 1990. Authigenesis of impact spheroids in the K/T boundary clay from Italy: New constraints for high-resolution stratigraphy of terminal Cretaceous events. *Journal of Sedimentary Petrology* 61:315–339.

Morgan et al.

Schulte P. 2003. The Cretaceous-Paleogene transition and Chicxulub impact ejecta in the northwestern Gulf of Mexico: Paleoenvironments, sequence stratigraphic setting, and target lithologies. Ph.D. thesis, University of Karlsruhe, Karlsruhe, Germany.

Scotese C. R., Gahagan L. M., and Larson R. L. 1988. Plate tectonic reconstructions of the Cretaceous and Cenozoic ocean basins. *Tectonophysics* 155:27–48.

Smit J. 1999. The global stratigraphy of the Cretaceous/Tertiary boundary impact ejecta. *Annual Review of Earth and Planetary Sciences* 27:75–91.

Smit J., Alvarez W., Montanari A., Swinburne N., Kempen T. M. V., Klaver G. T., and Lustenhouwer W. J. 1992. "Tektites" and microkrystites at the Cretaceous/Tertiary boundary: Two strewnfields, one crater? Proceedings, 23rd Lunar and Planetary Science Conference. pp. 87–100.

Stinnesbeck W., Schulte P., Lindenmaier F., Adatte T., Affolter M., Schilli L., Keller G., Stüben D., Berner Z., Krama U., Burns S. J., and Oliva J. G. L. 2001. Late Maastrichtian age of spherule deposits in northeastern Mexico: Implication for Chicxulub scenario. *Canadian Journal Earth Sciences* 38:229–238.

Stöffler D., Artemieva N., Ivanov B., Hecht L., Kenkmann T., Schmitt R., Tagle R., and Wittman A. 2004. Origin and emplacement of the impact formations at Chicxulub, Mexico, as revealed by the ICDP deep drilling Yaxcopoil-1 and by numerical modeling. *Meteoritics & Planetary Science* 39:???–???.

Swisher C. C., III, Nishimura J. M. G., Montanari A., Pardo E. C., Margolis S. V., Claeys P., Alvarez W., Smit J., Renne P., Maurasse F. J. M. R., Curtiss G., and McWilliams M. 1992. Coeval $^{40}Ar/^{39}Ar$ ages of 65.0 million years ago from Chicxulub crater melt-rock and Cretaceous-Tertiary boundary tektites. *Science* 257:954–958.

Zachos J. C., Arthur M. A., and Dean W. E. 1989. Geochemical evidence for suppression of pelagic marine productivity at the Cretaceous/Tertiary boundary. *Nature* 337:61–64.